Modelling of DC-DC Converters Based on Front-to-Front Connected MMC for Small Signal Studies

Abel A. Taffese*, Elisabetta Tedeschi**
Norwegian University of Science and Technology
Department of Electric Power Engineering
Trondheim, Norway
*abel.taffese@ntnu.no, **elisabetta.tedeschi@ntnu.no

Erik C. W. de Jong
Eindhoven University of Technology
Department of Electrical Engineering
Eindhoven, The Netherlands
e.c.w.de.jong@tue.nl

***Abstract*—The Multi-terminal DC grid is expected to be built incrementally by interconnecting existing HVDC installations. In doing so, an enabling component is the DC-DC converter which also plays the role of a power flow controller. A number of DC-DC converter topologies, targeting different applications, have been proposed in literature. However, detailed simulation models for system level studies are not developed, yet. This paper will focus on reduced order modelling and control of the Front-to-Front MMC based DC-DC converter for system level studies. The developed model is validated against a full detail average model. A simple approach to investigate poorly damped oscillations is also proposed. The approach is then used to investigate a poorly damped mode in the leg energy state that was excited by a transient in ac power.**

Keywords— DC-DC Converter, HVDC, F2F, Small Signal, state space

I. INTRODUCTION

A hybrid AC/DC grid is foreseen to be the future of the electric power system where the AC and DC grids complement each other [1]. Since AC grids are well established, a substantial research activity has been geared towards identifying and solving the major challenges of DC grids. Research groups, such as the Cigré's Study-Committee B4, have produced a handful of significant results identifying the challenges and demonstrating the feasibility of a DC grid [2]. One such challenge is control of power-flow in the grid. The Cigré working group B4.58 has been investigating devices and methods to overcome this challenge. Among the solutions proposed is the use of DC-DC converters. The DC-DC converter can also be an enabling component to connect existing point-to-point HVDC installations, such as those found in The North Sea, which are otherwise incompatible due to difference in operating voltage [3], grounding scheme or converter technology [4]. Despite its vital role, this DC-DC converter application has not been researched in depth, yet. A set of high-level requirements for such DC-DC converters was outlined in [3]. Different topologies, that fulfil these requirements for a specific application, have been proposed in literature [5]. This calls for the development of new models for power system studies, such as small signal analysis. Such system level studies are performed to investigate interactions between components, which are individually designed and optimized, when they are put together forming a larger system, such as the grid. Currently, very simplified, generic models are being used for such studies [6]. This choice is justified by magnitude of the system under those types of studies. However, ref. [7] discusses the shortcomings of using simplified models in system level studies which might lead to erroneous conclusion. Therefore, the models should be simplified in such a way that they do not loose important system information, such as poorly damped modes. Consequently, the DC-DC converters, like other components in the system, should be represented with proper level of detail in order to obtain accurate results from system level studies.

This paper presents simplified modelling and control of a specific kind of DC-DC converter for small signal stability studies: Front to Front (F2F) connected MMC. A small signal model for MMC has recently been developed for stability studies [8]. However, unlike [8], the topology considered in this

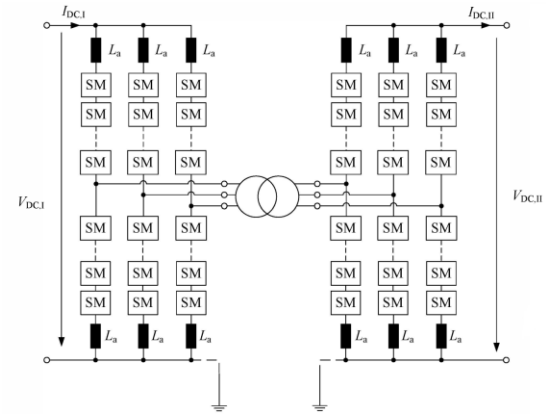

Fig. 1 F2F MMC based DC-DC Converter [4]

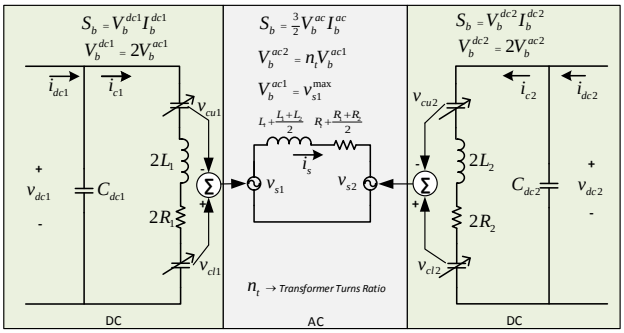

Fig. 2 Equivalent Model of the F2F Converter

Table 1 Main system parameters

Base Power, S_b	100 *MVA*	DC base voltage, V_b^{dc}	100 *kV*
AC base voltage, V_b^{ac}	50 *kV*	Number of cells, *N*	100
DC resistance, r_{dc}	0.0037	AC resistance, r_{ac}	0.04
DC inductance, l_{dc}	1.7×10^{-6}	AC inductance, l_{ac}	1.0×10^{-4}
H_{dc}	25 *ms*	H_{arm}	1 *ms*

work has two converters, which lead to peculiarities, such as interaction between the states of the two converters that affect the model simplification choices. The main contribution of this work is the development of a reduced order state-space small signal model and design of controllers for the aforementioned topology. The remainder of this paper is organized as follows. Section II briefly introduces the topology followed by derivation of the state space mode in section III. Section III.C presents simplifications to the model resulting reduced order model of the F2F, which is the main contribution of this paper. A control design approach for the leg energy is proposed in section IV. Section V presents simulation results that are used to validate the modelling assumptions. An approach to investigate and reduce poorly damped oscillations in the system is presented in section V.C.

II. Topology

As previously mentioned, a number of converter topologies have been proposed recently. Among these topologies, the F2F connected MMC-based DC-DC converter will be studied in this work. This converter was found to be suitable for medium voltage ratio (between 1.5 and 5) high voltage applications [9] making it a good candidate for HVDC transmission applications. The topology is shown in Fig. 1 where the two MMCs are coupled on the ac side via a transformer. The transformer provides voltage stepping functionality in addition to isolation between the two sides. The AC side is run at frequencies higher than the standard 50/60 Hz in order to benefit from the reduced footprint and initial investment [9]. For this study, the frequency is chosen to be 350 Hz which provides good tradeoff between the losses and footprint for offshore HVDC applications where space is a premium [9]. Table 1 presents main parameters of the system. H_{arm} and H_{dc} are inertia time constants of the arm and dc capacitances respectively. The respective capacitances are $c_x = 2H_x$. The per unit values are calculated on the bases given in Appendix A. For the sake of simplicity, the two MMCs are given the same parameters. However, the model derivation considers the general case with different parameters. The transformer turns ratio does not affect the per unit derivation. Therefore, it is assumed to be equal to one.

III. Model Development

A step by step derivation of a simplified average model of the F2F will be presented in this section. Equivalent circuit of the converter, shown in Fig. 2, is used for the derivation. For the purpose of modelling, the circuit is divided into dc and ac sides indicated by the colored regions. These two sides are coupled by the insertion index and the arm voltage. The circuit shows only one phase for simplicity. The two dc sides are represented by currents entering the converter. The dc capacitance represents the equivalent capacitance of the dc cable and submodule capacitors inserted. The arm voltage is represented by a variable capacitor in the figure. The ac side includes the equivalent arm inductance and transformer leakage in series with the respective resistances. The following simplifying assumptions are made.

- Proper low level voltage balancing control is in place.
- Compensated modulation is used [9].
- Since the ac side is entirely internal to the converter, it is assumed to be symmetric and balanced.
- Additionally, phase angle information is assumed to be accessible for the controller because the reference to the ac voltage is generated inside the controller. Therefore, it is assumed that a PLL is not required for the converter operation.

With these assumptions in place, the system dynamics can now be derived. Per phase quantities are presented for each signal. Using the given per unit base values, dynamics of the ac and dc sides will be derived followed by simplifications.

A. AC Side

With the two MMCs connected on the ac side, the ac equivalent circuit is given by two voltage sources connected with an R-L impedance. Therefore, the dynamic ac equation transformed to *dq* reference frame is given by (1).

$$\frac{l_{ac}}{2}\frac{di_{s1}^{dq}}{dt} = v_{s1}^{dq} - v_{s2}^{dq} - \frac{r_{ac}}{2}i_{s1}^{dq} - \omega \cdot l_{ac} \cdot J \cdot i_{s1}^{dq} \qquad J = \begin{bmatrix} 0 & -1 \\ 1 & 0 \end{bmatrix} \tag{1}$$

Where r_{ac} and l_{ac} are the equivalent, per unit, ac parameters.

B. DC Side

The dc link voltage is governed by (2), which shows that it is influenced by the dc current injected to the model and the circulating current in each leg. Since the dc side circuits are similar, the forthcoming derivation will only show the quantities of side 1.

$$c_{dc1}^{*}\frac{dv_{dc1}}{dt} = i_{dc1} - \sum_{k} i_{c1k}, \quad k \in \{\mathrm{a},\mathrm{b},\mathrm{c}\} \tag{2}$$

c_{dc1}^{*} is the equivalent capacitance of inserted submodules and other capacitance connected to the dc link. Similarly, the circulating current dynamics is given in (3).The subscript *k* will be used to denote per phase quantities.

$$l_{dc1}\frac{di_{c1k}}{dt} = v_{c1k} - r_{dc1}i_{c1k} \tag{3}$$

where r_{dc1}, l_{dc1}, i_{c1k}, and v_{c1k} are arm resistance, arm inductance, circulating current, and voltage across the arm impedance, respectively, in per unit with dc base values. The

remaining part of the dc dynamics is the arm voltage which is given by (4). v_{cu1k}^{Σ} and v_{cl1k}^{Σ} are the upper and lower arm voltages, respectively.

$$\begin{aligned}\frac{c_1}{N_1}\frac{dv_{cu1k}^{\Sigma}}{dt} &= n_{u1k}i_{u1k}\\ \frac{c_1}{N_1}\frac{dv_{cl1k}^{\Sigma}}{dt} &= n_{l1k}i_{l1k}\end{aligned} \tag{4}$$

n_{u1k} and n_{l1k} are insertion indices of each arm. i_{u1k} and i_{l1k} are currents of the upper and lower arms respectively. The basic equations relating insertion indexes and arm voltages is given in (5) together with the arm current relations.

$$\begin{aligned}n_{u1} &= \frac{v_{dc1}-v_{s1}-2v_{c1}}{2v_{cu1}^{\Sigma}} \text{ and } n_{l1} = \frac{v_{dc1}+v_{s1}-2v_{c1}}{2v_{cl1}^{\Sigma}}\\ i_{u1} &= i_{c1}+\frac{2}{3}i_{s1} \quad \text{and} \quad i_{l1} = i_{c1}-\frac{2}{3}i_{s1}\end{aligned} \tag{5}$$

Where v_{s1} and i_{s1} are the phase voltage and current, respectively. With (4), the average MMC model is now complete. This model will be the reference model and henceforth, it will be referred to as *Model 1*. For this model to be useful in small signal stability studies, it has to be linearized. However, some of the model variables, arm voltages, have oscillating values in steady state making it impossible to linearize the model. One way to achieve constant values in steady state is to simplify the model ignoring the oscillating components [9]. The next section deals with the simplifications that can be applied to obtain a linear model.

C. Simplifications

As a first step, the arm voltages in a leg can be decomposed into sum, v_{c1k}^{Σ}, and difference, v_{c1k}^{Δ}, components shown by (6).

$$\begin{aligned}\frac{c_1}{N_1}\frac{dv_{c1k}^{\Sigma}}{dt} &= n_{u1k}i_{u1k}+n_{l1k}i_{l1k}\\ \frac{c_1}{N_1}\frac{dv_{c1k}^{\Delta}}{dt} &= n_{u1k}i_{u1k}-n_{l1k}i_{l1k}\end{aligned} \tag{6}$$

From (6), it can be seen that the two components cannot be separated without making simplifying assumptions. This is because of the fact that the insertion index involves division by arm voltages. However, if the arm energy dynamics is considered instead of the voltage, the two components can be separated. With proper choice of base values [9], the arm energy, in per unit, can be made equal to the square of the arm voltage. After substitution of arm currents and insertion indices from (5), the upper and lower arm energies are given in (7) in per unit to the aforementioned base value.

$$\begin{aligned}\frac{dw_{cu1}}{dt} &= \frac{N_1}{c_1}\left(v_{dc1}i_{c1}-2v_{c1}i_{c1}-\frac{2}{3}v_{s1}i_{s1}+\frac{2}{3}v_{dc1}i_{s1}-v_{s1}i_{c1}-\frac{4}{3}v_{c1}i_{s1}\right)\\ \frac{dw_{cl1}}{dt} &= \frac{N_1}{c_1}\left(v_{dc1}i_{c1}-2v_{c1}i_{c1}-\frac{2}{3}v_{s1}i_{s1}-\frac{2}{3}v_{dc1}i_{s1}+v_{s1}i_{c1}+\frac{4}{3}v_{c1}i_{s}\right)\end{aligned} \tag{7}$$

From (7), the sum, w_1^{Σ}, and difference, w_1^{Δ}, energies of the arms in a given leg are given in (8).

$$\begin{aligned}\frac{dw_1^{\Sigma}}{dt} &= \frac{2N_1}{c_1}\left(v_{dc1}i_{c1}-2v_{c1}i_{c1}-\frac{2}{3}v_{s1}i_{s1}\right)\\ \frac{dw_1^{\Delta}}{dt} &= \frac{2N_1}{c_1}\left(\frac{2}{3}v_{dc1}i_{s1}-v_{s1}i_{c1}-\frac{4}{3}v_{c1}i_{s1}\right)\end{aligned} \tag{8}$$

From (8), it can be seen that the sum component is dependent on the average power transfer between the ac and dc sides. The difference part, on the other hand, is a result of power flowing back and forth between the arms in a leg. For the purpose of power system studies, it is shown to be sufficient to consider only the sum component [9]. This assumption results in a significant simplification in the MMC model. This leads to the fact that all the arms in the MMC can be aggregated in to one state. The model implementing this assumption will be referred to as *Model 2* in the coming discussions.

Model 2 is an F2F counterpart of what was proposed in [9]. The aggregate leg energy equation in terms of three phase active power, for the two MMCs, is given in (9). p_1 and p_2 are ac active powers output by the two MMCs. If the losses in the ac side are ignored, the two power terms will be equal in magnitude and opposite in sign. This fact will be exploited to obtain further simplifications.

$$\begin{aligned}\frac{3c_1}{2N_1}\frac{dw_1^{\Sigma}}{dt} &= 3\left(v_{dc1}-2v_{c1}\right)i_{c1}-p_1\\ \frac{3c_2}{2N_2}\frac{dw_2^{\Sigma}}{dt} &= 3\left(v_{dc2}-2v_{c2}\right)i_{c2}-p_2\end{aligned} \tag{9}$$

The two energy terms in (9) can be decomposed into common mode and differential terms in a fashion similar what was done previously for the arm energy. This results in (10) where w_{ave} and w_{Δ} are the common mode and differential terms, respectively. From (10), it can be seen that the common mode term is affected by dc power balance between the two dc sides while the differential term is related to power balance between the ac and dc sides. The energy controllers control the common mode term. Therefore, if these controllers are properly designed, the common mode term can be assumed to be equal to the reference value given by (12). This reduces the energy states to one for the whole converter. The arm energies of the two sides can then be recalculated from (11). The model implementing this assumption will be referred to as *Model 3*.

$$\begin{aligned}\frac{3c_1}{N_1}\frac{dw_{ave}}{dt} &= 3\left(v_{dc1}-2v_{c1}\right)i_{c1}+3\left(v_{dc2}-2v_{c2}\right)i_{c2}\\ \frac{3c_1}{N_1}\frac{dw_{\Delta}}{dt} &= 3\left(v_{dc1}-2v_{c1}\right)i_{c1}-3\left(v_{dc2}-2v_{c2}\right)i_{c2}-2p_1\end{aligned} \tag{10}$$

$$w_{ave} = \frac{w_1+\eta w_2}{2}, \quad w_{\Delta} = \frac{w_1-\eta w_2}{2}, \text{ and } \eta = \frac{c_2N_1}{c_1N_2} \tag{11}$$

$$w_{ave}^{*} = \frac{w_1^{*}+\eta w_2^{*}}{2} \tag{12}$$

Model 3 is linearized, using MATLAB, around an operating point in order to be used in system stability analysis. The linear model will be called *Model 4*. Fig. 3 shows block diagram of *Model 4* where the dc currents are input and the output is dc voltage. The four different models are summarized in Table 2.

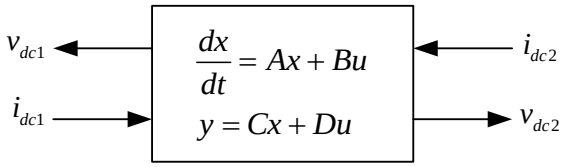

Fig. 3 Block representation of *Model 4*

The assumption made in this section will be verified when the models are validated in section V.B.

Table 2 Summary of Models

Model Name	Description	No. of equations
Model 1	Full detail average model	22
Model 2	Single arm per MMC	8
Model 3	Single arm per F2F	7
Model 4	Linearized model	7

IV. Control Design

This section details controller design aspects for the F2F. There are different levels of controller that are required for proper operation of an MMC [9]. At the highest level, there are generic current and power controllers that are topology-independent. These controllers are implemented in Synchronous Frame Reference (SFR) *dq* reference frame [10]. One of the MMCs plays the role of a slack bus by producing a specified ac voltage while the second one controls active and reactive power injection. These controllers are tuned using modulus optimum technique [11] since the plant models do not include integrators. At a lower level, there are energy and circulating current controllers that are specific to MMCs. A proposed design approach for the energy controller is presented in the next section.

A. Energy Control

From (9), it can be seen that the average arm energy can be controlled by using circulating current. Assuming that the change in energy due to circulating current is significantly larger the other terms and $v_{dc} >> v_c$, a linear representation of the plant, together with the controllers, can be derived as shown in Fig. 4. Two measurement filters are included in the block diagram to represent filters and measurement delays. The inner circulating current controller is used to control the energy. Since steady state error is removed by the outer controller, the inner loop can be of P type. The closed loop performance specification with such a controller is given by (13).

$$\omega_n^2 = \frac{1+\frac{k_p}{r_{dc}}}{\tau_{dc}\tau_{fi}} \quad \text{and} \quad \zeta = \frac{\tau_{dc}+\tau_{fi}}{\tau_{dc}\tau_{fi}}\frac{1}{2\omega_n} \tag{13}$$

Where ζ and ω_n are desired closed loop damping and natural frequencies, respectively. It can be seen that controller can only control one of the two parameter. Had the controller been of PI type, the two parameters would have been controlled independently. However, for the purpose of the system under consideration, the P type controller can be sufficient [12]. The desired damping is chosen as a design objective resulting in (14), where k_p is the proportional constant. The damping was chosen to be 0.707 in order to achieve a good dynamic response.

$$k_p = r_{dc} \times \left[1 - \left(\frac{\tau_{dc}+\tau_{fi}}{2\zeta}\right)^2 \frac{1}{\tau_{dc}\tau_{fi}}\right] \tag{14}$$

By ignoring the second order term, the following first order model can approximate the resulting closed loop circulating current transfer function.

$$\frac{1}{\tau_{eqi}s+1} \quad \text{where } \tau_{eqi} = \frac{2\zeta}{\omega_n} \tag{15}$$

The outer loop plant transfer function becomes:

$$\frac{w_f(s)}{i_c^*(s)} = \frac{2\bar{V}_{dc}N}{c}\frac{1}{s\left(\tau_{eqw}s+1\right)} \tag{16}$$

where $\tau_{eqw} = \tau_{fw} + \tau_{eqi}$ is a first order approximation of the two first order transfer function in the loop. $\bar{V}_{dc}$ is the nominal dc voltage. The energy controller is chosen to be PI type since reference tracking and disturbance rejection are desired properties. Looking at the structure of (16), symmetrical optimum technique is well suited for the tuning of the energy controller. The following values are calculated using the given system parameters. k_{pw} and k_{iw} are proportional and integral constants of the energy controller, respectively.

$$k_{pw} = \frac{c}{4\bar{V}_{dc}N \cdot \tau_{eqw}} \quad \text{and} \quad \mathrm{k}_{iw} = \frac{k_{pw}}{4\tau_{eqw}} \tag{17}$$

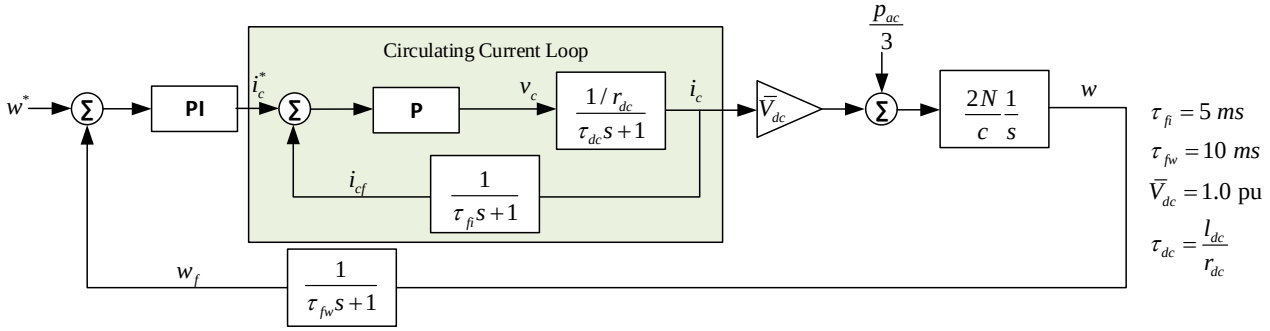

Fig. 4 Energy Controller Block Diagram

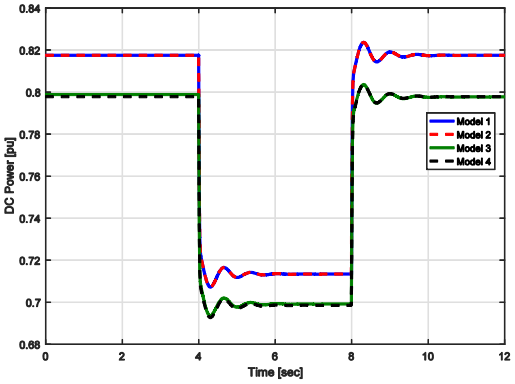

Fig. 5 Comparison of Models: DC Power

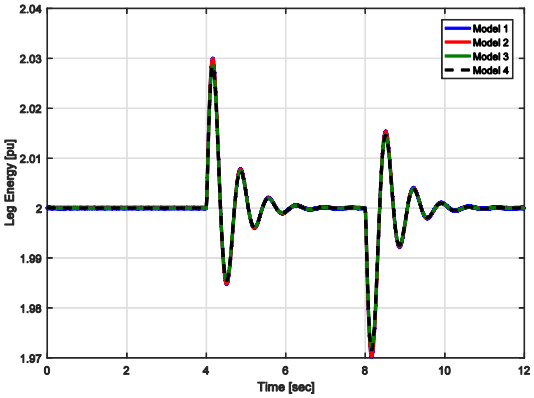

Fig. 6 Comparison of Models: Leg Energy

V. Simulation Results

Simulation results and analysis are presented in this section. The first section describes the simulation setup while the second section deals with validation of the modeling assumptions and simplifications that were made in preceding sections. The last section proposes a linear analysis approach to study and troubleshoot oscillation problems in the system.

A. Simulation Setup

The model of Fig. 2 is connected to two droop controlled dc voltage sources on the two sides. Although the derivation was general, for the sake of simplicity, the per unit values of parameters for the two MMCs are taken to be equal. The ac voltage is 0.85 pu. The reference to ac power is a square wave signal with maximum and minimum amplitudes of 0.8 and 0.7 pu, respectively.

B. Model Validation

DC power and leg energy measurements are used to quantitatively compare the simplified models to the reference, *Model 1*. Three measurement indices are used to indicate goodness of the model in reproducing the reference signals. The first measure is relative absolute error in percentage calculated using (18).

$$e_{abs}[\%] = \sum_{n} \frac{|x_{1n} - x_{mn}|}{|x_{1n}|} \times 100, \ \ \mathrm{m} \in \{2,3,4\} \qquad (18)$$

Where x_1 and x_m are signals from the reference and simplified models respectively. The second indicator is offset error to quantify any dc error. The third value is correlation which shows how closely the two signals change together. The later two can provide more information about the source of a given error. Simulation results are shown in Fig. 5 and Fig. 6.

Table 3 Modelling Errors: DC Power

	Model 2	*Model 3*	*Model 4*
Absolute Error	0.0042	0.0198	0.0203
Offset Error	0	-0.0092	-0.0092
Corr. Coefficient	1.00	0.999	0.999

Table 4 Modelling Errors: Leg Energy

	Model 2	*Model 3*	*Model 4*
Absolute Error	4.36e-04	1.05	1.18
Offset Error	0	0	0
Corr. Coefficient	1.00	1.00	1.00

As can be seen from the results, *Model 2* closely follows *Model 1*'s output. Modelling errors are depicted in Table 3and Table

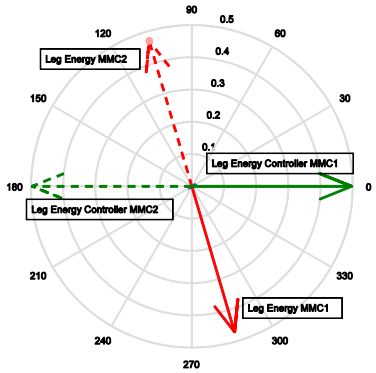

Fig. 8 Observability of Mode 15

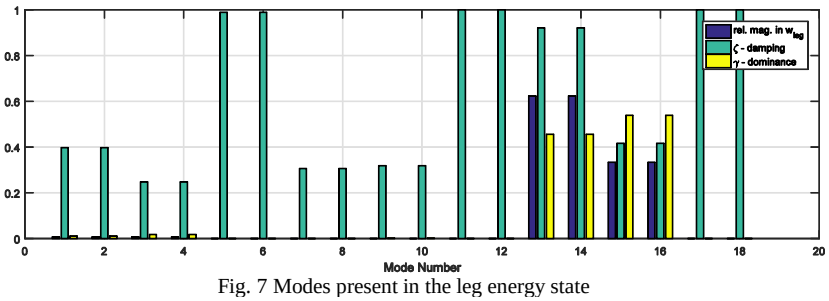

Fig. 7 Modes present in the leg energy state

4.There is a dc offset error in the dc power of Models 3 and 4 due to the fact that the losses are ignored in the simplification. The correlation coefficients show that the waveforms change in the same way despite of the clearly visible offset in the dc power. From these results, it can be concluded that the simplified model can be used to accurately represent the reference model.

From Fig. 6, it can be noticed that the waveform exhibits an oscillatory response while the controller was designed with a goal of achieving good damping. This phenomenon is investigated in detail in the next section.

C. Linear Analysis

Since the model validation in previous section showed that the simplified models reproduce *Model 1* with good fidelity, linear analysis on *Model 4* can be used to study the oscillation that was observed. The basic setup of a state space model is given in (19) .

$$\frac{dx}{dt} = Ax + Bu \qquad (19)$$
$$y = Cx + Du$$

where *x* is the state variable, *y* is the output, and *u* is the input. The state variables can be seen as a combination of the modal variables. Modal variables or modes are a set of simple responses that characterize the system. The relative quantities of different modes present in a given state are given by the residues [13], r_{ijk} ,of the given mode with the selected state as output as shown in (20).

$$r_{ijk} = c_j \times w_i \times v_i \times b_k \qquad (20)$$

Where $i, j, and\ k$ are indexes of the mode, state, and input, respectively. b and c are input and output vectors, respectively. w_i and v_i are the left and right eigenvectors of mode i . With this information, one can identify which mode is causing the oscillation. Once the mode is identified, the next step is to see the presence of that mode in all the states to understand the nature and type of the mode. This can be done by looking at the right eigenvector. The last step is to understand the mode and take remedial actions.

Since the oscillation is observed in the energy state, the residue of modes contributing to leg energy, together with their respective damping, are plotted in Fig. 7. In order to identify the dominant modes, the factor γ was introduced to serve as a simple measure of visibility of a given mode in the output (or state). It is the ratio of residue to damping of a given mode. High value of γ implies that the mode dominates the response. Therefore, from Fig. 7, the dominant modes in the leg energy state are modes 15 and 16, which are complex conjugates. From the observability plot of mode 15, Fig. 8, it can be seen that the two energy controllers are working in opposite directions. The damping of these modes was found to be influenced by the bandwidth of the circulating current controllers. Therefore, one way to counteract the oscillation is to make the circulating current controller faster. This can be done by reducing damping of the closed loop circulating current transfer function, given by (13). Simulation results with damping reduced to 0.4 (originally 0.707) is shown in Fig. 9. The oscillation is now sufficiently damped. Other methods, such as power oscillation damping controllers can also be used if increasing the bandwidth of circulating current control is not feasible.

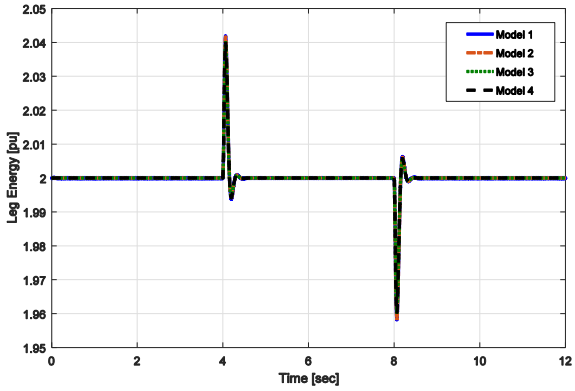

Fig. 9 Improved damping in leg energy state

VI. Conclusion

A reduced order small signal model of the F2F DC-DC converter was developed in this paper. The modeling assumptions and simplifications were validated against a full detail model. Absolute error, dc offset, and correlation indices are used to quantify modelling error incurred by each of the simplified models. A step by step controller design approach based on approximate transfer functions was also presented. Simulation results indicated that there are poorly modes in the system that were not originally considered in the control design process. These modes resulted in an oscillatory response, especially in the arm energy. Linear analysis was used to identify these modes and provide the necessary additional damping. Unlike the simplified models that are currently used to present DC-DC converters, the model developed in this paper captures the converter dynamics with good accuracy compared to the full detail model. Therefore, it can be integrated into multi-terminal or meshed dc grid models for stability studies.

Appendix

A. Per Unit Base Values

The following values are chosen as per unit base. The given choice of base values for the inductance and capacitance is equivalent to setting the base frequency, ω_b , to 1. This will simplify the differential equations and preserve the formula for computing time constants when converting to per unit.

$$I_b^{ac} = \frac{2S_b}{3V_b^{ac}} \quad Z_b^{ac} = \frac{V_b^{ac}}{I_b^{ac}} \quad L_b^{ac} = Z_b^{ac} \quad C_b^{ac} = \frac{1}{Z_b^{ac}}$$
$$I_b^{dc} = \frac{S_b}{V_b^{dc}} \quad Z_b^{dc} = \frac{V_b^{dc}}{I_b^{dc}} \quad L_b^{dc} = Z_b^{dc} \quad C_b^{dc} = \frac{1}{Z_b^{dc}} \qquad (21)$$

REFERENCES

[1] Y. Yang, M. Jafar, P. Vaessen, A. Yanushekvich, Y. Fu, R. Marshall, T. Bosma, and M. Irvine, "Hybrid Grid: Towards a Hybrid AC/DC Transmission Grid," DNV GL Strategic Research & Innovation, Position Paper, 2015.

[2] B. Andersen, "HVDC Grids - Overview of CIGRE Activities and Personal Views," CIGRE SC-B4, 2014.

[3] C. Barker, C. Davidson, D. Trainer, and R. Whitehouse, "Requirements of DC-DC Converters to facilitate large DC Grids," *Cigre Session 2012*, 2012.

[4] A. Schon and M.-M. Bakran, "High power HVDC-DC converters for the interconnection of HVDC lines with different line topologies," in *Power Electronics Conference (IPEC-Hiroshima 2014 - ECCE-ASIA), 2014 International*, 2014, pp. 3255–3262.

[5] G. P. Adam, I. A. Gowaid, S. J. Finney, D. Holliday, and B. W. Williams, "Review of dc–dc converters for multi-terminal HVDC transmission networks," *IET Power Electronics*, vol. 9, no. 2, pp. 281–296, 2016.

[6] M. K. Zadeh, M. Amin, J. A. Suul, M. Molinas, and O. B. Fosso, "Small-signal stability study of the Cigré DC grid test system with analysis of participation factors and parameter sensitivity of oscillatory modes," in *Power Systems Computation Conference (PSCC), 2014*, 2014, pp. 1–8.

[7] M. Amin, J. A. Suul, S. D'Arco, E. Tedeschi, and M. Molinas, "Impact of state-space modelling fidelity on the small-signal dynamics of VSC-HVDC systems," in *AC and DC Power Transmission, 11th IET International Conference on*, 2015, pp. 1–11.

[8] G. Bergna Diaz, J. A. Suul, and S. D'Arco, "Small-signal state-space modeling of modular multilevel converters for system stability analysis," in *Energy Conversion Congress and Exposition (ECCE), 2015 IEEE*, 2015, pp. 5822–5829.

[9] T. Luth, M. M. C. Merlin, T. C. Green, F. Hassan, and C. D. Barker, "High-Frequency Operation of a DC/AC/DC System for HVDC Applications,"*IEEE , Transactions on Power Electronics* vol. 29, no. 8, pp. 4107–4115, 2014.

[10] S. D'Arco, J. A. Suul, and O. B. Fosso, "Small-signal modeling and parametric sensitivity of a virtual synchronous machine in islanded operation," *International Journal of Electrical Power & Energy Systems*, vol. 72, pp. 3–15, 2015.

[11] C. Bajracharya, M. Molinas, J. A. Suul, T. M. Undeland, and others, "Understanding of tuning techniques of converter controllers for VSC-HVDC," in *Nordic Workshop on Power and Industrial Electronics (NORPIE/2008), June 9-11, 2008, Espoo, Finland*, 2008.

[12] L. Harnefors, A. Antonopoulos, S. Norrga, L. Angquist, and H.-P. Nee, "Dynamic analysis of modular multilevel converters," *IEEE Transactions on Industrial Electronics*, vol. 60, no. 7, pp. 2526–2537, 2013.

[13] M. I. Garcıa Planas and J. L. Domınguez Garcıa, "A general approach for computing residues of partial-fraction expansion of transfer matrices," WSEAS transactions on mathematics, vol. 12, no. 7, pp. 647–756, 2013.